Stability of real-time MR temperature mapping in healthy and diseased human liver

Claudia Weidensteiner, Noureddine Kerioui, Bruno Quesson, Baudouin Denis de Senneville, Hervé Trillaud, Chrit Moonen

Stability of real-time MR temperature mapping in healthy and diseased human liver

Claudia Weidensteiner[1], PhD, Noureddine Kerioui[1,3], MD, Bruno Quesson[2], PhD, Baudoin Denis de Senneville[1], Hervé Trillaud[1,3], MD, Chrit T.W. Moonen[1], PhD.

[1]Laboratory for Molecular and Functional Imaging: From Physiology to Therapy CNRS/Université Victor Segalen Bordeaux 2, Bordeaux, France;

[2]Image Guided Therapy SA, Pessac, France;

[3]Service de Radiologie, St. André Hospital, CHU Bordeaux, Bordeaux, France.

Original Research

Running title: stability of MR temperature mapping in human liver
Word count: 5277

Address correspondence to:
Dr. Chrit Moonen
IMF CNRS/Université Victor Segalen Bordeaux 2
146, rue Léo Saignat, Case 117
33076 Bordeaux,France

Phone : ++33-5-5757 4586, Fax : ++33-5-5757 4597
Email : moonen@imf.u-bordeaux2.fr

Grants: Marie Curie stipend of the European Union for C.W.
La Ligue National Contre le Cancer
Philips Medical Systems
Conseil Régional d'Aquitaine

Abstract

Purpose: To determine the stability and quality of MR temperature mapping using the proton resonance frequency (PRF) method in the liver of hepatic tumor patients.

Material and Methods: The standard deviation of a series of temperature maps was determined in 30 patients (21 cirrhotic livers with carcinoma, 9 non-cirrhotic livers with metastasis or angioma) and in 5 volunteers at normal body temperature under free breathing. A respiratory-gated segmented EPI sequence (3 slices in 1 expiration phase) was performed with SENSE acceleration on a 1.5 T scanner. Motion corrupted images were identified by calculation of the cross-correlation coefficient and discarded.

Results: A T_2^* range of 10-33 ms was found with especially low values in advanced cirrhotic livers. The mean temperature standard deviation in patients was 2.3°C (range 1.5-5.0°C). The stability in healthy livers was slightly better than that in cirrhotic livers, and it was higher in the right than in the left liver. The gaiting failed in 4 % of the images when the respiratory cycle was irregular, leading to motion artifacts and errors in the temperature maps.

Conclusion: The achieved temperature stability and image quality makes real-time quantitative monitoring of thermal ablation of liver tumors feasible on a clinical scanner.

Keywords: MRI, temperature mapping, liver, Sensitivity Encoding, Proton Resonance Frequency

Introduction

Minimally invasive, percutaneous ablative therapies under image guidance with thermal energy sources such as radio frequency (RF), and laser are increasingly used for tumor ablation in the clinic because of their efficacy and low cost. Ultrasound (US) or CT imaging is used for positioning the RF needle or laser fiber. However, a precise and quantitative on-line control of the ablation is not possible with these imaging modalities. The imaging method used for clinical guidance should ideally have a good spatial, temporal, and thermal resolution and should be easily implemented. In addition, the thermal and spatial resolution should be sufficient to detect temperature rise in the tissue around the lesion in order to 1) enable real-time control of the ablation of the complete tumor and of a safety margin of 5 - 10 mm around the tumor and to 2) avoid unwanted thermal damage in healthy tissue.

MRI can monitor temperature changes quantitatively using the temperature-dependent shifts of the proton resonance frequency (PRF) ([1]) or the temperature dependency of T_1 ([2]). Therefore temperature mapping with MRI can be used to predict the treatment outcome during the heating procedure. T_1-weighted sequences have been used in clinical trials of thermal ablation in the liver ([3],[4],[5]). However, calibration of the method is difficult due to non-linear effects when coagulation occurs. Therefore, quantitative temperature mapping for ablation procedures is difficult with T_1-methods. The PRF-method has proven to be precise at a field strength $\geq$ 1 T ([6]) when based on RF-spoiled, gradient echo imaging. The PRF change is linear with temperature and independent of tissue type when fat suppression is applied. Its disadvantage is the sensitivity to motion artifacts, since the method is based on the phase difference between two complex MR images. For mobile organs, such as the liver, motion may induce erroneous temperature mapping and therefore, motion correction has to be applied. Preliminary accounts of PRF-based temperature mapping in the human liver has recently been reported based on the following motion correction methods: 1) respiratory

triggering or gating ([7]); 2) the use of motion insensitive sequence like radial scanning ([8]). In addition, suspension of respiration has been applied under general anesthesia to improve temperature mapping ([9]). The latter approach may not be feasible due to the patient's condition.

Fast imaging sequences have to be applied for real-time control because they are less sensitive to respiratory motion artifacts and allow gated acquisition in the expiration phase. However, the PRF-method is most sensitive if TE is in the same range as T_2^* ([10]) which is rather short in the healthy liver (20 – 30 ms). Additionally, T_2^* of the liver may vary depending on the pathology. Therefore, the duration of the EPI echo-train in fast gradient-echo sequences has to be limited to obtain an accurate temperature estimate. A possibility to shorten acquisition time is the use of partial parallel acquisition techniques like SENSE ([11]) with the use of a phased array coil. The SENSE technique has previously been used for imaging of moving objects like the heart ([12]). Phase maps acquired with SENSE techniques have not yet been reported for temperature mapping.

In a recent paper ([13]) we have shown that PRF temperature mapping can be successfully performed in healthy rabbit liver in vivo during laser ablation. A segmented gradient echo EPI sequence with fat suppression, respiratory gating, and flow suppression was performed. Based on those results, the method was adapted for human liver. In order to prepare clinical trials on image-guided ablation of human liver tumors, the quality of temperature mapping should be tested under clinical conditions.

The aim of this work was to investigate the stability of PRF temperature mapping on a clinical scanner in the liver of volunteers and liver tumor patients. The stability was assessed by measuring the standard deviation of a series of temperature maps at baseline temperature, i.e. the tissue was not heated and not ablated. For a given TE, the phase stability can be directly correlated with temperature stability. Respiratory gating was combined with the rapid

acquisition scheme of a SENSE segmented EPI-sequence to improve motion correction. The key questions of this study were the following: 1) Is the stability of the method sufficient to obtain reliable temperature information with measurement uncertainty of a few °C (small compared to the temperature increase needed for ablation studies)? 2) Can the method be performed in liver tumor patients suffering from cirrhosis or steatosis? 3) Is the performance different in patients with cirrhotic livers (having primary tumors) than in patients with healthy livers (having secondary tumors)?

Materials and Methods

Patient and Volunteer Handling

Five healthy volunteers and thirty patients were recruited for this temperature mapping study under an approved study protocol. The patients were divided in 2 groups: 1) cirrhotic livers (21 patients with hepatocellular carcinoma (HCC)) and 2) non-cirrhotic livers (7 patients with liver metastases: 4 from colorectal tumor, 2 from neuroendocrine tumor, 1 from gastric tumor; 2 patients with angioma). One patient of the first and four patients of the second group had liver steatosis. Four patients of the first group had advanced cirrhosis. A total of 35 imaging sessions was performed in the first group, since many patients were scanned more than once. Twenty-six of all patients underwent ultrasound guided RF ablation of liver tumors several weeks before this study. Their written consent was received before the start of the protocol. The volunteers and patients were lying supine with a flexible 4-element phased array body coil (standard equipment; Philips Medical Systems, Best, The Netherlands) wrapped around their chest. A respiratory sensor (standard equipment; Philips Medical Systems, Best, The Netherlands) was positioned between their chest and the coil for continuous monitoring of breathing and respiratory gating of the sequence. The volunteers

and patients were allowed to breathe freely (respiratory cycle duration approx. 4 sec) during temperature mapping.

Hepatic T_2^* was determined in 3 healthy volunteers and in 11 patients (9 patients with HCC due to cirrhosis; 1 patient with HCC due to hemachromatosis; 1 with a healthy liver and a benign tumor) with the same phased array coil as described above. One volunteer and one patient with cirrhosis were scanned twice. The measurement was performed in one breath hold of 15 sec duration.

MR Protocol for Temperature Mapping

MR experiments were performed on two 1.5 T Philips Intera clinical scanners (Philips Medical Systems, Best, The Netherlands) using the built-in quadrature body coil for excitation and a 4-element phased array flexible body coil for signal detection. For comparison, additional experiments were performed in 10 patients for which the quadrature body coil was used for both excitation and detection.

In the volunteer experiments without SENSE acceleration, a segmented EPI sequence with 9 gradient echoes (EPI-factor 9) and TE/TR of 16 ms/119 ms was used (TE range 6.1 ms – 23.7 ms). The FOV was 300 mm x 300 mm to 350 mm x 350 mm (depending on the size of the abdomen); and the matrix was 112 x 90 (zerofilled to 128 x 128), yielding an in-plane resolution of 2.7 mm x 3.3 mm to 3.1 mm x 3.9 mm. Three parallel slices (thickness 5 mm, gap 6 mm) were acquired in an interleaved mode within one respiratory cycle gated at the end of expiration (acquisition time 1.2 sec). The phase encoding direction was the left-right direction. Since fat does not show a temperature dependent frequency shift fat signal must be suppressed to avoid an erroneous temperature map. This is especially important in the liver. Thus, a water-selective binomial spectral-spatial excitation pulse (25° flip angle) was applied for slice selection, as was described previously ([14]). Two parallel saturation slabs (thickness 60

mm, gap 8 mm) were used to suppress flow artifacts. For comparison, protocols without saturation slabs with the same spatial resolution were acquired (TR shortened to 100 ms). Data were collected with just one coil element of the array (the one closest to the liver), and also with all 4 elements.

A SENSE acceleration factor of 1.5 and 2 was performed using acquisition parameters described above. The acquisition time was reduced to 0.79 sec for SENSE factor 1.5 and to 0.60 sec for SENSE factor 2, due to partial acquisition of k-space.Before the start of the temperature mapping protocol a sensitivity map of the phased array coil was acquired to allow SENSE reconstruction and reconstruction of the phase map from the phased array data.

For the patient studies, a segmented EPI sequence as described above was used, but with only 7 gradient echoes and TE/TR of 12 ms/119 ms (TE range 5.9 ms – 16.4 ms). The FOV was 300 mm x 300 mm to 400 mm x 400 mm (depending on the size of the abdomen); and the matrix was 112 x 89 (zerofilled to 128 x 128), yielding an in-plane resolution of 2.7 mm x 3.3 mm to 3.6 mm x 4.5 mm. The slices were placed at the original tumor position in each patient. Data were collected with all 4 receiver coil elements. A SENSE acceleration factor of 1.5 was used. In addition, images with an EPI-factor of 9, and with TE=16 ms, were acquired for the patient group with healthy liver. A reference map of the coil sensitivity was acquired before the start of the temperature mapping protocol. A FOV of 500 mm x 500 mm and a matrix size of 144 x 112 (zerofilled to 256 x 256) were employed for the experiments using the built-in quadrature body coil for excitation and signal detection, yielding a nominal in-plane resolution of 3.5 mm x 4.5 mm. TE/TR was 16 ms/119 ms; EPI-factor was 7. The gating width was 1200 ms, resulting in a time resolution of 3 slices in 2 respiratory cycles.

Data Processing

Reconstruction of magnitude and phase MR images was done on-line using the standard Philips hard- and software available on clinical scanners. Analysis of stability and performance of the method was performed off-line in the IDL program environment (Research Systems Inc., Boulder, CO, USA). To obtain a temperature map, the phase map was subtracted from a reference phase map (which was checked to be free of severe motion artifacts), yielding the phase difference $\Delta\Phi$ in each point r . After phase unwrapping, the temperature difference ΔT was calculated according to

$$\Delta T(\vec{r}) = \frac{\Delta\Phi(r)}{\alpha \cdot TE \cdot \gamma \cdot B_0}, \qquad (1)$$

where $\alpha = -0.0101 \pm 0.0004\, ppm/°C$ ([15]) is the temperature dependant water chemical shift, γ is the gyromagnetic ratio, and B_0 is the field strength.

In order to identify motion-corrupted images, the cross-correlation was calculated between the magnitude reference image and each of the magnitude images in a time series of 20 images based on the following formula

$$P_{XY} = \frac{\sum_{k=0}^{N-1}(X_k - \overline{X})(Y_K - \overline{Y})}{\sqrt{\left[\sum_{k=0}^{N-1}(X_k - \overline{X})^2\right]\left[\sum_{k=0}^{N-1}(Y_k - \overline{Y})^2\right]}} \qquad (2)$$

where P_{XY} is the cross-correlation coefficient of 2 images X and Y with k is the number of the pixel for a total of N pixels (=128x128 pixels). $\overline{X}, \overline{Y}$ are the mean image signal intensities. The calculation was performed for the complete image, not just for a part of it. When the cross-correlation coefficient was lower than 0.95 (experimentally determined threshold), the image was considered as corrupted and therefore discarded.

To determine the noise level of the temperature maps, the standard deviation of the phase in each pixel was calculated for the series of 20 phase maps (of 1 slice) in volunteers

and patients. The standard deviation was only calculated for those time series where 0 or 1 image was discarded because of motion problems. A temperature standard deviation map was calculated from the resulting phase standard deviation map with equation 1. The temperature standard deviation was averaged in 3 regions of interest (ROI): the complete liver, left liver, and in the right liver. The signal-to-noise-ratio SNR was determined in the magnitude images with following formula ([16])

$$SNR = \frac{S}{\sigma_N \cdot 1.53}. \qquad (3)$$

The signal amplitude S was averaged in a region without vessels in the liver in one slice and the standard deviation of the noise σ_N was determined in a region outside the body.

MR Protocol and Post Processing for T_2^* Measurement

MR experiments were performed with the standard body coil for excitation and the 4 elements phased array flexible body coil for signal detection as described above. A set of 9 gradient echo images was acquired in one breath-hold to observe T_2^* decay in the liver using a segmented EPI sequence, with TR=150 ms and TE ranging from 9.2 ms to 50.8 ms. Two adjacent, transversal slices of 6.5 mm thickness with a FOV of 420 mm x 223 mm and a matrix size of 256 x 99 were acquired, yielding an in-plane resolution of 1.6 mm x 2.3 mm. Phase encoding was performed in the anterior–posterior direction. A water-selective binomial spectral-spatial excitation pulse was applied for slice selection, as was described previously (Erreur : source de la référence non trouvée). A ROI was chosen in the liver on the image series and the signal intensity was averaged in the ROI for each TE. An exponential decay was fitted to the time evolution of signal intensity, yielding T_2^*.

Results

T_2^* Determination

T_2^* in livers with early cirrhosis was in the range of 17 – 31 ms (mean ± SD = 23.8 ± 5.3 ms; n=9) and not significantly different from healthy livers (patient with benign tumor and volunteers) where the range was 23 - 33 ms (mean ± SD = 27.1 ± 3.9 ms; n=5). In advanced cirrhosis and in hemochromatosis, T_2^* is significantly shorter, with values as low as <10 ms. Its precise value could not be determined with the used sequence, since TE of the used sequence is too long for such short T_2^* values. As a consequence, we generally reduced TE and echo train duration for temperature mapping in patients compared to volunteers to improve temperature stability and SNR.

Stability of the Method in Volunteers

Both phase and magnitude images acquired without saturation slabs show flow artifacts in the phase direction around the big vessels. With saturation slabs, the flow artifact vanishes and the vessels appear dark in the magnitude images. Note that the gall bladder still appears bright. The MR temperature mapping shows higher precision when using the saturation slabs: the temperature standard deviation map has lower values and is more homogeneous throughout the liver. The temperature standard deviation maps show a standard deviation of 1 – 3 ˚C in most parts of the liver. Areas with standard deviation > 5˚C are restricted to regions with residual movement artifacts, like regions close to the stomach and the chest wall. As expected, more severe motion artifacts were observed when the phase encoding direction was changed to anterior-posterior, the main direction of breathing motion

The average value for the standard deviation for all volunteers was lower for EPI without SENSE, than for EPI with SENSE (Table 1). The SENSE magnitude images show a lower SNR for higher SENSE factors. Theoretically a decrease to $1/\sqrt{1.5} = 82\%$ and

$1/\sqrt{2} = 71\%$ is expected for an acceleration factor of 1.5 and 2, respectively (Erreur : source de la référence non trouvée). The experimental SNR values reported in Table 1 were found to be in good agreement with theory. Temperature stability was not determined for SENSE factors > 2, since reconstruction artifacts hampered the image quality. The breathing cycle length in the healthy volunteers is sufficient to acquire 3 slices even without SENSE within one cycle. However, this is not possible with a shorter breathing cycle length. Then SENSE acceleration is recommended to acquire all 3 slices within one breathing cycle.

Additionally, experiments with the same sequence, the same coil and identical parameters as for human liver in vivo were performed on a heated beef liver sample to verify the accuracy of the SENSE method for temperature mapping in comparison with absolute temperature measurement with a thermocouple. The MR thermometry corresponded well with classical thermometry. The standard deviation of MR thermometry was less than 0.5°C for beef liver ex vivo.

Stability of the Method in Patients

Figure 1 shows the magnitude image, the phase image, and the color-coded map of the temperature standard deviation for 3 patients with cirrhosis, severe cirrhosis, and metastasis of colorectal cancer, respectively. The image quality in all 3 patients is sufficient to obtain phase information over the complete abdomen, despite the significantly lower signal intensity in severe cirrhotic liver than in non-cirrhotic or slightly cirrhotic livers. Residual motion artifacts can be seen in a large number of patients for liver tissue adjacent to the stomach showing up as red area in the standard deviation map (Fig 1, bottom row middle). Consequently the temperature standard deviation in the left liver was higher than in the right liver (Table 2).

The SNR in the liver was in the range of 60 - 100. In livers with severe cirrhosis (n=4), the SNR in the liver was approximately 40% lower than the SNR in the spleen. SNR was in the same range for non-cirrhotic (healthy or steatose) or slightly cirrhotic livers.

There was no difference in temperature standard deviation between livers with and without steatosis in the group of the non-cirrhotic livers (Table 2). In the other group, the standard deviation of patients with advanced cirrhosis was only calculated in 2 of the 4 patients (mean of standard deviation in total liver 3.03°C and 1.65°C), since too many images were corrupted for two of these patients. The patient with cirrhosis and steatosis did not show a significantly different standard deviation compared to the mean value in this group.

The stability depends also on the position of the slice. A slice in the dome of the liver shows more artifacts than a centered slice, because of the stronger influence of the respiratory motion or even by heart motion. A slice in the base of the liver can be corrupted by stomach or bowel motion.

The images obtained with the built-in quadrature body coil showed, as expected, a decrease in SNR of 68 % (n=8) due to the lower sensitivity of this coil (Fig. 3). Nevertheless, the image quality was sufficient to obtain stable phase maps. The stability was lower compared to the measurements with the 4-element body coil in the same patients: the mean temperature standard deviation was 0.49 °C higher with the quadrature body coil (n=8). The spatial resolution is decreased since a larger FOV is needed to avoid back folding of the images of arms. In addition, the temporal resolution was lower (2 respiratory cycles) using the same gating width, since no SENSE acceleration can be performed

A reduction of the gating window from 1200 ms to 600 ms (consequently causing a reduction of the temporal resolution from 1 to 2 respiratory cycles) did not improve the results for patients with short, irregular breathing cycles. Another option to reduce the gating width without a reduction in time resolution was the use of SENSE factor 2. Under these

experimental conditions, the gating width was 900 ms and the stability of the method was slightly improved. The SNR decreased in accordance with the volunteer experiments.

An increase of echo time from 12 ms to 16 ms (with an increase of the echo train length from 7 to 9) in the patient group with non-cirrhotic livers (where slightly longer T_2^* values were found) resulted in a decrease of the temperature standard deviation by 0.32°C (n=6), whereas a decrease of the mean SNR with echo time could not be observed in this subgroup.

Identification of motion-corrupted images

Irregular breathing caused failure of the gating method leading to 2 kinds of artifacts: 1) Breathing during the acquisition in the gating window time span lead to motion-corrupted images showing the typical ghosting and blurring in the phase encode direction (intra-images artifacts). 2) Irregular breathing depths changed the position of the image plane by through-plane motion (Fig. 2 bottom). Motion artifacts caused peaks in the range of 8 – 20 °C in the time evolution of the temperature difference in one voxel. Those motion-corrupted images were automatically identified with the cross-correlation algorithm. The images with a cross-correlation coefficient < 0.95 corresponded to the images with artifact peaks in the temperature difference curve (Fig. 2, top). They were discarded from the time series of images. After the identification step the temperature difference curve displays no data at the specific time point. The number of discarded images was determined in each image time series (Table 3). In 83 % of the patients with cirrhosis no or one image was corrupted, compared to 89 % of the patients without cirrhosis patients and 100 % of the volunteers. However, in the patients with advanced cirrhosis, this number drops to 50%., In total, only 4% of temperature maps were found to be corrupted of all images acquired with SENSE factor 1.5 in patients and volunteers.

A change in echo time did not change significantly the number of corrupted images in patients with healthy livers (Table 4). However, the number increased when using the built-in body coil for signal acquisition. A reduction of the acquisition window by decreasing the time resolution increased the number of corrupted images, whereas use of SENSE factor 2 led to a reduction of the number of motion-corrupted images.

Discussion

T_2^* Values

It has been previously shown that the sensitivity of the PRF method has a maximum for TE=T_2^*. However, hepatic T_2^* is rather short (compared to e.g. kidney or brain tissue), leading to the following consequences for temperature mapping sequences: 1) The echo train duration in the segmented EPI-sequence must be limited, since TE should not exceed T_2^*. The shorter the echo train length, the more TR periods are needed to complete an image and the longer is the total acquisition time. 2) The spatial resolution is hampered since a rapid T_2^* decay broadens the point spread function which determines the actual voxel size. Therefore, quantitative temperature mapping using PRF is more challenging in the liver than in other organs.

The T_2^* value depends on the local field homogeneity and it can therefore differ for the same patient/volunteer from scanner to scanner or from session to session. Thus, tissue of the same type can have a wide range of T_2^* values as is also shown in our measured values. We did not determine accurate T_2^* calculations n a patient with liver metastasis, since in general signal intensity (and hence T_2^*) is not different from healthy tissue of healthy volunteers. However, this is not the case for a liver with steatosis, which may lead to different T_2^* . The tissue changes in patients with early cirrhosis did not result in a significant change in T_2^* as compared to healthy livers. However, in livers with advanced cirrhosis T_2^* dropped under 10

ms. In the case of hemachromatosis, the hepatic T_2^* below 10 ms can be explained by the iron deposits resulting from this pathology. To cover a broad range of T_2^* values with the same sequence (without having to measure T_2^* in every patient), we reduced TE and echo train length as compared to the initial volunteer experiments. This reduction does not lead to a significant reduction in quality of MR temperature mapping in patients with non-cirrhotic livers (like in the volunteer experiments) since an increase in TE and echo train length did not significantly improve the temperature stability.

Patient Study

The stability of the method is sufficient to obtain reliable temperature information in patients with a measurement standard deviation of 3°C or less. The precision of temperature estimate is highly dependent on both the SNR and the influence of motion on acquired images. An estimate of the influence of the SNR can be easily obtained by looking at the quality of the magnitude images. In case of an insufficient SNR, acquisition parameters have to be changed. By analyzing the correlation factor it is possible to evaluate the performance of the respiratory gating. When the percentage of corrupted images is too high, the gating parameters have to be adapted.

The motion correction method using simple respiratory gating was sufficient, and the SENSE acceleration can be very useful in patients who exhibit a short and irregular breathing cycle. The method can be easily implemented on a clinical scanner since only standard equipment is used. The post processing is not time-consuming, so that temperature difference maps can be obtained in real time using the previously described software interface ([17],[18]). The obtained temperature difference maps are quantitative and thus allow immediate control and adjustment of the laser or RF energy deposition offering the possibility of an automatic feedback control loop (Erreur : source de la référence non trouvée). The accuracy of the

respiratory-gated PRF-method for monitoring laser ablation was shown previously in rabbit liver in vivo (Erreur : source de la référence non trouvée).

The main contribution to the residual error of the method is the motion of the liver in vivo that, apparently, cannot be prevented by the respiratory gating. In comparison, a much smaller standard deviation (approximately 0.5°C) can be achieved with this method on a static beef liver sample ex vivo.

In many patients, the temperature standard deviation was higher than 10°C in liver tissue close to the stomach. The reason for this is slight motion of that liver segment caused by digestive movements of the stomach. A possible solution for temperature monitoring in this region would be the use of medication reducing digestive motion during the procedure.

Images corrupted by irregular breathing motion could be successfully identified and discarded on the basis of cross-correlation of the magnitude images with a threshold of 0.95. Due to the high temporal resolution of the method of a single breathing cycle the loss of temperature information at a single time point does not significantly hamper the quality of the monitoring of a typical ablation procedure with a duration of 15 - 30 min. A fixed cross-correlation threshold value, emerically determined, appeared a simple and effective solution. Other thresholds are also possible, e.g. based on the standard deviation of the cross-correlation coefficient. The calculation of the cross-correlation is fast and easy, and thus can be implemented in a real-time software interface. It should be noted that the image intensity may change in the heated zone due to T_1 changes in an ablation experiment. As a consequence, it is recommended to exclude this area in cross-correlation calculations in the case of high local change of the contrast.

The number of discarded images is a measure for the performance of the respiratory gating method. In 84% of the patients the method performed well (only 5% or less of the images were corrupted), in only 7% of the patients more than 25% of the images were

corrupted. In cases of very short breathing cycles, the number of corrupted images could be lowered and the stability could be improved by the use of a smaller gating window width. This was either achieved by using a higher SENSE factor (however, SENSE factors > 2 caused artifacts); or by keeping the SENSE factor at 1.5, leading to a decreased time resolution (2 instead of 1 breathing cycles). In our study, the first method lead to better results. At the present status of the visualization algorithms, the corrupted images were simply discarded and no post-processing for motion artifact correction was employed. If needed, a suitable correction method can be developed to enable on-line correction of in-plane motion thus conserving the temperature information.

The images acquired with the built-in body coil showed a large decrease in SNR (due to the coil geometry and the loading factor), which lead to significantly lower temperature stability. In addition, SENSE acceleration cannot be used with this coil. However, the stability remains sufficient for temperature monitoring. The advantage is the better accessibility to the patient. With the wrap-around phased-array coil the catheter with the laser fiber or the RF-needle needs to be placed through the openings of this coil thus limiting access.

When comparing the two patient groups, the temperature stability was slightly higher in the patients without cirrhosis. In the case of the advanced cirrhotic livers, this can be explained by the lower SNR compared to healthy livers, since the SNR is affecting the phase standard deviation and therefore the stability of the method ([19]). In our study, a higher number of cirrhotic than non-cirrhotic patients had an irregular breathing cycle causing possible failure of the respiratory gating.

General anesthesia is often applied during an ablation procedure leading to a more regular and slowerbreathing, possibly resulting in an improved performance of the gating method. In case of a conscious sedation of the patient, the respiration is also slightly more regular than in the freely breathing patients of this study without any sedation. Nevertheless,

the current study performed with patients and volunteers breathing freely - which can be considered as more challenging in this respect – the stability of real time temperature mapping was judged to be sufficient for guidance of ablation procedures since the temperature standard deviation is much lower than the absolute temperature difference during the procedure while maintaining a temporal resolution much higher than the total heating duration.

Conclusion

The proposed method using a respiratory gated segmented EPI sequence with SENSE has a high temperature stability, a high temporal and a sufficient spatial resolution for accurate monitoring of temperature during thermal ablation. The SENSE method is particularly suited for short respiratory cycles due to the reduced acquisition time. The results of this study indicate that quantitatively monitoring ablation procedures in the liver using real-time temperature mapping is feasible using conventional clinical MR instrumentation. Monitoring of temperature for both healthy and cirrhotic livers of all stages should be possible with a temporal resolution of a single respiratory cycle and a spatial resolution of 3-4 mm both under general anesthesia and conscious sedation.

Acknowledgements

The authors thank Bénédicte Caire-Gana for her help with the volunteer experiments. This work was presented at the 11th annual meeting of the ISMRM in Toronto

[1] Ishihara Y, Calderon A, Watanabe H, Mori K, Okamoto K, Suzuki Y, Sato K, Kuroda K, Nakagawa N, Tsutsumi S. A precise and fast temperature mapping method using water proton chemical shift. In: Proceedings of SMRM, 11th Annual Meeting, Berlin, 1992. p. 4803.

[2] Dickinson RJ, Hall AS, Hind AJ, Young IR. Measurements of changes in tissue temperature using MR imaging. J Comput Assist Tomogr 1986;10:468-472.

[3] Vogl TJ, Muller PK, Hammerstingl R, Weinhold N, Mack MG, Philipp C, Deimling M, Beuthan J, Pegios W, Riess H, et al. Malignant liver tumors treated with MR imaging-guided laser-induced thermotherapy: technique and prospective results. Radiology. 1995;196:257-265.

[4] Fiedler VU, Schwarzmaier HJ, Eickmeyer F, Muller FP, Schoepp C, Verreet PR. Laser-induced interstitial thermotherapy of liver metastases in an interventional 0.5 Tesla MRI system: technique and first clinical experiences. J Magn Reson Imaging. 2001;13:729-737.

[5] Dick EA, Joarder R, de Jode M, Taylor-Robinson SD, Thomas HC, Foster GR, Gedroyc WM. MR-guided laser thermal ablation of primary and secondary liver tumours. Clin Radiol 2003;58:112-120.

[6] Quesson B, de Zwart JA, Moonen CT. Magnetic resonance temperature imaging for guidance of thermotherapy. J Magn Reson Imaging 2000;12:525-533.

[7] Morikawa S, Inubushi T, Kurumi Y, Naka S, Seshan V, Tsukamoto T. Feasibility of simple respiratory triggering in MR-guided interventional procedures for liver tumors under general anesthesia. In: Proceedings of ISMRM, 10th Annual Meeting, Hawaii 2002. p. 2240.

[8] Schaeffter T, Weiss S, Rasche V. Radial MRI – a motion insensitive temperature mapping method. In: Proceedings of ISMRM, 9th Annual Meeting, Glasgow 2001. p. 325.

[9] Morikawa S, Inubushi T, Kurumi Y, Naka S, Sato K, Tani T, Yamamoto I, Fujimura M. MR-guided microwave thermocoagulation therapy of liver tumors: Initial clinical experiences using a 0.5 T open MR system. J Magn Reson Imaging. 2002;16:576-583.

[10] De Zwart JA, van Gelderen P, Kelly DJ, Moonen CT. Fast magnetic-resonance temperature imaging. J Magn Reson B 1996;112:86-90.

[11] Pruessmann KP, Weiger M, Scheidegger MB, Boesiger P. SENSE: sensitivity encoding for fast MRI. Magn Reson Med 1999;42:952-962.

[12] Pruessmann KP, Weiger M, Boesiger P. Sensitivity encoded cardiac MRI. J Cardiovasc Magn Reson 2001;3:1-9.

[13] Weidensteiner C, Quesson B, Caire-Gana B, Kerioui N, Rullier A, Trillaud H, Moonen CTW. Real-time MR temperature mapping of rabbit liver in vivo during thermal ablation. Magn Reson Med, *in press*

[14] De Zwart JA, Vimieux FC, Delalande C, Canioni P, Moonen CTW. Fast lipid suppressed MR temperature mapping with echo-shifted gradient echo imaging and spectral-spatial excitation. Magn Reson Med 1999;42:53-59.

[15] Peters RD, Hinks RS, Henkelman RM. Ex-vivo tissue type independence in proton-resonance frequency shift MR thermometry. Magn Reson Med 1998;40:454-459.

[16] Kaufman L, Kramer DM, Crooks LE, Ortendahl DA. Measuring signal-to-noise ratios in MR imaging. Radiology 1989;173:265-267.

[17] Vimeux FC, de Zwart JA, Palussière J, Fawaz R, Delalande C, Canioni P, Grenier N, Moonen CTW. Real-time control of focused ultrasound heating based on rapid MR thermometry. Invest Radiol 1999;34:190-193.

[18] Salomir R, Vimeux FC, de Zwart JA, Grenier N, Moonen CT. Hyperthermia by MR-guided focused ultrasound: accurate temperature control based on fast MRI and a physical model of local energy deposition and heat conduction. Magn Reson Med 2000;43:342-347.

[19] Conturo TE, Smith GD. Signal-to-noise in phase angle reconstruction: dynamic range extension using phase reference offsets. Magn Reson Med 1990;15:420-437.

Table 1

	without SENSE	SENSE 1.5	SENSE 2
temperature standard deviation in °C	1.38 ± 0.33	2.03 ± 0.55	1.93 ± 0.63
relative SNR	1	0.87 ± 0.32	0.74 ± 0.25

Table 1: **Temperature stability and SNR in volunteers (n=5).**

The values of the temperature standard deviation maps were averaged over the total liver, the mean value in °C is shown for the respiratory gated segmented EPI sequence without SENSE, with SENSE factor 1.5, and with SENSE factor 2. The SNR values are calculated relative to the value obtained without SENSE.

Table 2

	total liver	left liver	right liver
cirrhotic livers (n=29)	2.34 ± 1.13	3.14 ± 2.93	2.07 ± 0.87
non-cirrhotic livers (n=8)	2.18 ± 0.92	2.80 ± 1.38	1.97 ± 0.84
steatosis (n=4)	2.15 ± 1.26	2.18 ± 1.59	2.11 ± 1.11
healthy (n=4)	2.21 ± 0.63	3.42 ± 0.94	1.82 ± 0.61

Table 2: **Temperature stability in patients.**

The values of the temperature standard deviation maps were averaged in the total liver, the left, and the right liver. The mean values for all images series with less than 2 corrupted images are shown. All values are mean ± standard deviation in °C.

Table 3

Number of corrupted images	0-1	2-5	≥ 6
volunteers (n=5)	5	0	0
cirrhotic livers (n=35)	29	4	2
non-cirrhotic livers (n=9)	8	0	1

Table 3: **Number of motion-corrupted images in a time-series of 20.**

The images were acquired with the 4-channel coil and SENSE factor 1.5. An image was defined as corrupted when its cross-correlation coefficient > 0.95.

Table 4

Number of corrupted images	0-1	2-5	≥ 6
built-in body coil (n=10)	8 (10)	1 (0)	1 (0)
2 respiratory cycles (n=6)	5 (4)	0 (2)	1 (0)
SENSE 2 (n=8)	7 (6)	1 (1)	0 (1)
TE=16ms, non-cirrhotic livers (n=7)	6 (7)	1 (0)	0 (0)

Table 4: **Number of motion-corrupted images in a time-series of 20 for different acquisition schemes.**

The images were acquired with the built-in body coil (without SENSE), with a shortened acquisition window and a temporal resolution of 2 respiratory cycles (SENSE 1.5), with a shortened acquisition window and SENSE 2, and with TE=16ms in patients with non-cirrhotic livers (SENSE 1.5). In brackets are the number of corrupted images acquired with the 4-channel coil, TE=16 ms, and SENSE factor 1.5 in the same patients. An image was defined as corrupted when its cross-correlation coefficient > 0.95.

Fig. 1: Transversal images in 3 liver tumor patients acquired with the respiratory-gated SENSE-EPI sequence, together with corresponding color-coded map of the temperature standard deviation of a time series of temperature maps.

Fig. 2: Time course of measured temperature difference in a single voxel for a patient with a healthy liver with metastasis (top left) together with cross-correlation coefficient for this series of images (top right). The horizontal dashed line represents the threshold value for the cross-correlation. The peak in the temperature difference curve corresponds to an image with cross-correlation coefficient < 0.95 (arrows). As can be seen on the 3 successive images of the time series (bottom), the temperature jump was caused by through-plane motion (arrow).

Fig. 3: Comparison between images (top row) and map of temperature standard deviation (bottom row) acquired with the built-in body coil (left column) and with the 4-channel coil (right column) in the same patient with a cirrhotic liver.

Fig. 1

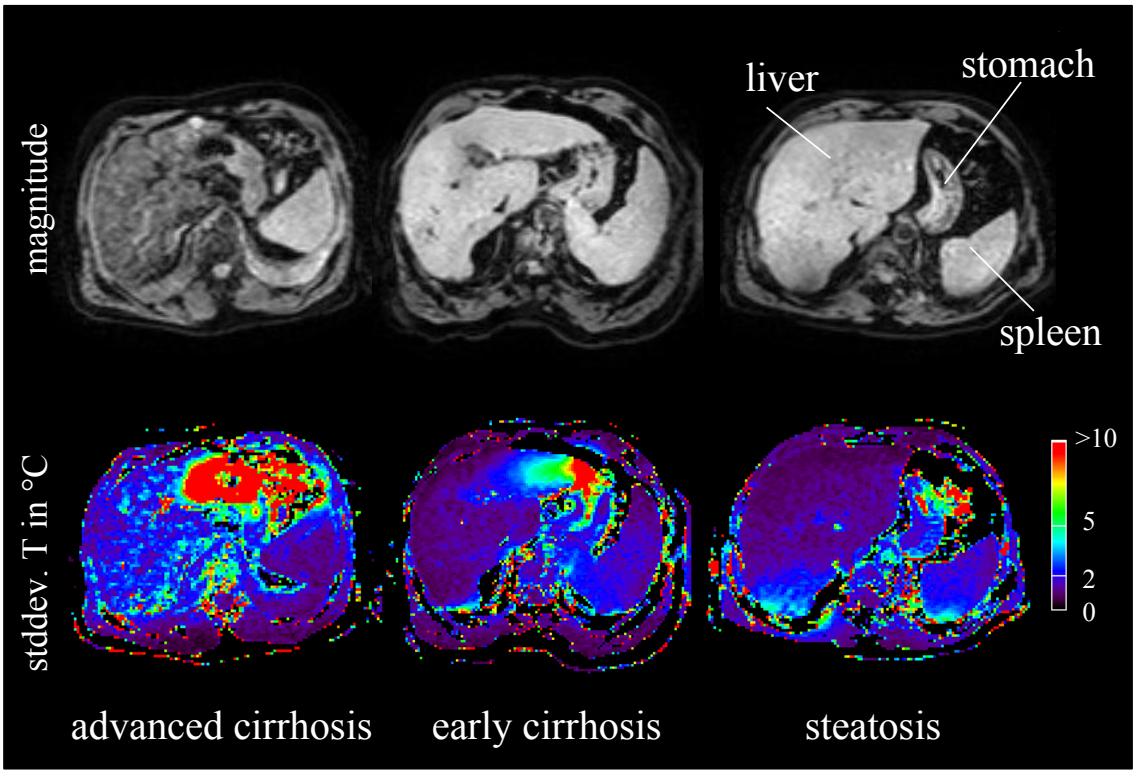
magnitude
liver
stomach
spleen
stddev. T in °C
>10
5
2
0
advanced cirrhosis
early cirrhosis
steatosis

Fig. 2

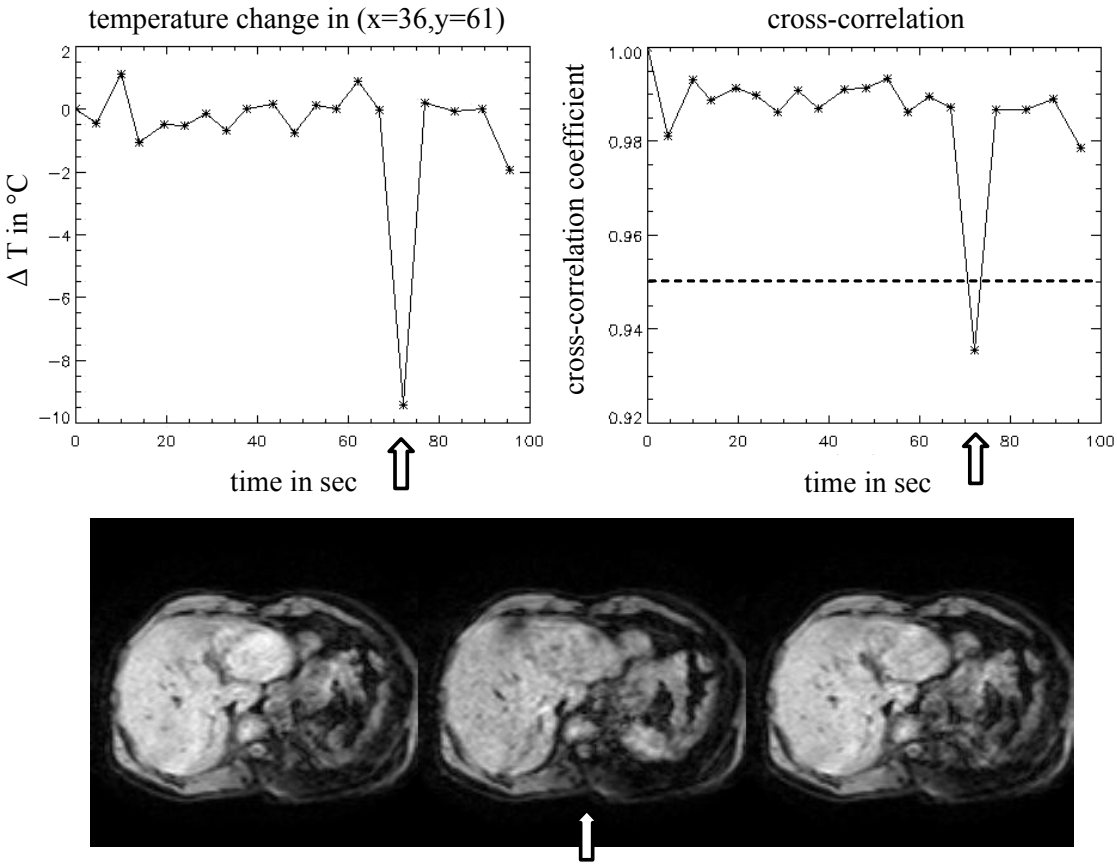
temperature change in (x=36,y=61)
Δ T in °C
time in sec
cross-correlation
cross-correlation coefficient
time in sec

Fig. 3